Suction Caissons & Vertically Loaded Anchors: Design Analysis Methods

By

Charles Aubeny, PhD and Don Murff, PhD
Department of Civil Engineering
Texas A&M University

Final Report on the Suction Caissons & Vertically Loaded Anchors: Design Analysis Methods

for the Project

Suction Caissons and Vertically Loaded Anchors

Prepared for the Minerals Management Service

Under the MMS/OTRC Cooperative Research Agreement

1435-01-99-CA-31003

Task Order 16169

1435-01-04-CA-35515

Task Order 35980

MMS Project Number 362

and

OTRC Industry Consortium

December 2005

OTRC Library Number: 12/05A162

For more information contact:

Offshore Technology Research Center
Texas A&M University
1200 Mariner Drive
College Station, Texas 77845-3400
(979) 845-6000

or

Offshore Technology Research Center
The University of Texas at Austin
1 University Station C3700
Austin, Texas 78712-0318
(512) 471-6989

A National Science Foundation Graduated Engineering Research Center

PREFACE

The project Suction Caissons and Vertically Loaded Anchors was conducted as series of inter-related studies. The individual studies are as follows:

- Suction Caissons & Vertically Loaded Anchors: Design Analysis Methods by Charles Aubeny and Don Murff, Principal Investigators
- Suction Caissons: Model Tests by Roy Olson, Alan Rauch and Robert Gilbert, Principal Investigators
- Suction Caissons: Seafloor Characterization for Deepwater Foundation Systems by Robert Gilbert Principal Investigator
- Suction Caissons: Finite Element Modeling by John Tassoulas Principal Investigator

This report summarizes the results of the Suction Caissons & Vertically Loaded Anchors: Design Analysis Methods study.

TABLE OF CONTENTS

LIST OF TABLES

LIST OF FIGURES

Suction Caissons & Vertically Loaded Anchors: Design Analysis Methods

Principal Investigators

Charles Aubeny and Don Murff

PROJECT OBJECTIVES

The project objectives are to (1) determine the currently available best practices for analysis and design of suction caisson anchors (SCA's) and vertically loaded anchors (VLA's) including drag embedment anchors, and (2) effect improvements in the installation and capacity predictions for SCA's and VLA's.

The overall research program for investigating anchor performance includes single experimental model tests, finite element analyses, and developing simplified design tools for practitioners. The TAMU researchers (PI's Aubeny and Murff) focused on simplified design tools for estimating the ultimate pullout capacity of anchors.

PROGRESS AND RESULTS – SUCTION ANCHORS

General Methodology

The general framework for development of the simplified formulations discussed herein is plastic limit analysis (PLA). PLA formulations can include upper and lower bound solutions. This research largely utilized an upper bound approach involving:

1. Postulating a kinematically admissible collapse mechanism.
2. Computing the rate of internal energy dissipation associated with that mechanism.
3. Equating the rate of internal energy dissipation to the rate of work due to externally applied loads to determine an upper bound estimate of load capacity.
4. Systematically optimizing the collapse mechanism to obtain a least upper bound estimate of load capacity.

Internal Energy Dissipation

The second step in the upper bound analyses involves evaluating the rate of internal energy dissipation associated with the postulated collapse mechanism. In the most rigorous approach, this involves four steps. First, strain rates at any point in the deforming soil surrounding the suction anchor are calculated by taking spatial derivatives

of velocity fields. Next, the corresponding stresses at any point in the soil mass are calculated by invoking a flow rule – associated flow rules in the case of the formulations considered in this paper. The product of strain rate and stress yields the rate of energy dissipation per unit volume. The total rate of energy dissipation is calculated by integrating –usually numerically - over the appropriate volume. Discontinuous velocity fields can also be accommodated in the analysis. Although strain rates across a slip plane are infinite, the rate of energy dissipation per unit surface area approaches a finite value as the volume of soil containing the slip plane becomes infinitesimally thin (Murff, 1980). In this case, the dissipation energy per unit area is integrated across the surface area of the slip plane.

The analysis described above can require considerable computational effort, as it requires evaluation of volume and surface integrals that can involve considerable complexity when three dimensional collapse mechanisms are considered. Further, even when simplifying assumptions are made regarding the collapse mechanism, optimizing the geometry of the mechanism to achieve a least upper bound solution is a complex problem in itself. In the case of the Murff and Hamilton (1993) analysis to be discussed subsequently, four optimization parameters are utilized in the search for a least upper bound solution for lateral load capacity. Considerable simplification of the PLA analysis is possible if the net effect of the three-dimensional stress field in the soil surrounding the caisson is expressed in terms of equivalent forces and moments acting on the caisson. This expedient greatly reduces the computational effort in evaluating the rate of energy dissipation – the dimension of the integrals reduces from three to one – and reduces the number of optimization variables describing the collapse mechanism. The resulting reduction in computational effort permits analyses that are well within the capabilities of spreadsheet programs, although the range of site conditions that can be considered by this simplified approach is more restrictive than the more rigorous solution methods.

The simplified analyses described above use a generalized plastic limit analysis (Prager, 1959) in which forces and moments are considered as ‘generalized stresses’, with velocities and rotation rates being the corresponding work conjugate ‘generalized strains’. In addition, for the case of suction anchors subjected to inclined loads, the interaction relationships between horizontal, vertical, and moment resistance can be

considered as a generalized yield surface. Therefore, by invoking an associated flow rule, velocities and rotation rates can be related to resisting forces and moments in the same manner that strain rates are related to stresses in conventional plasticity analyses.

PLA of a Laterally Loaded Suction Caisson

Figure 1 shows the starting point for this research, the collapse mechanism postulated by Murff and Hamilton (1993) for laterally loaded piles which is equally applicable to laterally loaded suction anchors. The mechanism comprises three regions: a surface failure wedge, a zone at depth in which the soil flows horizontally around the translating-rotating caisson, and a spherical failure surface at the caisson tip. Murff and Hamilton show that this collapse mechanism can be fully described in terms of four optimization parameters describing the rotation of the caisson (L_0) and the geometry and motions of the surface failure wedge. The optimal combination of these parameters leads to a least upper bound solution for suction anchor lateral load capacity. Lateral resistance calculated from the Murff-Hamilton approach compare favorably to the empirical relations of Matlock (1970) and Reese et al. (1975).

A substantial portion of this research involved simplification and modifications to the Murff-Hamilton solution to develop (1) a simplified solution for laterally loaded suction anchors, (2) a model for suction anchors subjected to combined vertical and horizontal loads, and (3) a model for suction anchor capacity in anisotropic soils.

Laterally Loaded Suction Caissons

Model Development

The Murff-Hamilton mechanism described above offers an effective but somewhat computationally intensive approach for estimating suction anchor lateral load capacity. In seeking a simpler design tool, an equivalent mechanism in Figure 2 was proposed for this research (Aubeny et al., 2000). The horizontal soil force per unit of caisson depth $H(z)$ is calculated from an empirical expression for side resistance proposed by Murff and Hamilton (1993) based on their analysis of the collapse mechanism in Figure 1. The important outcomes of this simplification are: (1) the computations involved in evaluating internal energy dissipation are greatly reduced, and (2) the collapse mechanism involves only a single optimization variable (L_0), greatly simplifying the

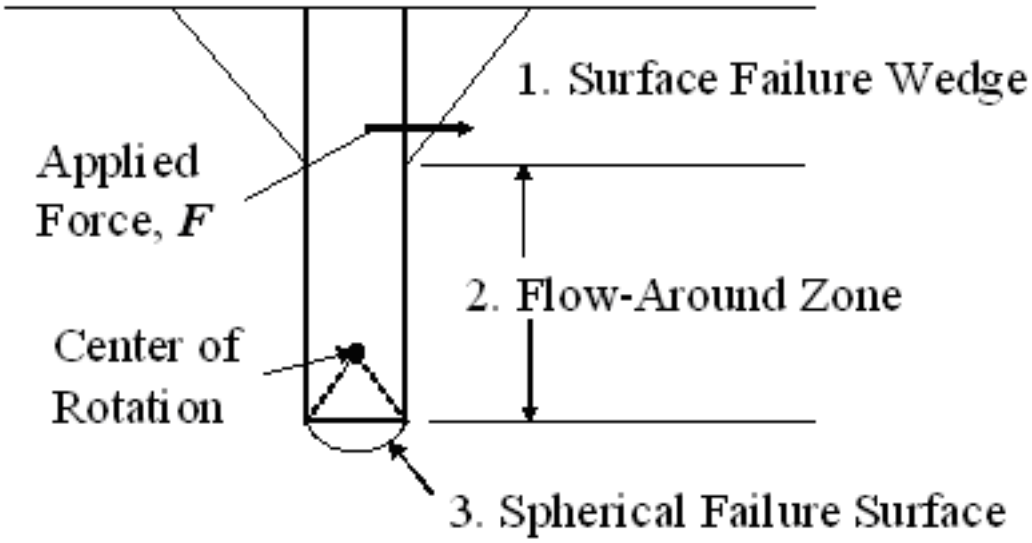

Figure 1. Failure Mechanism Assumed by Murff and Hamilton

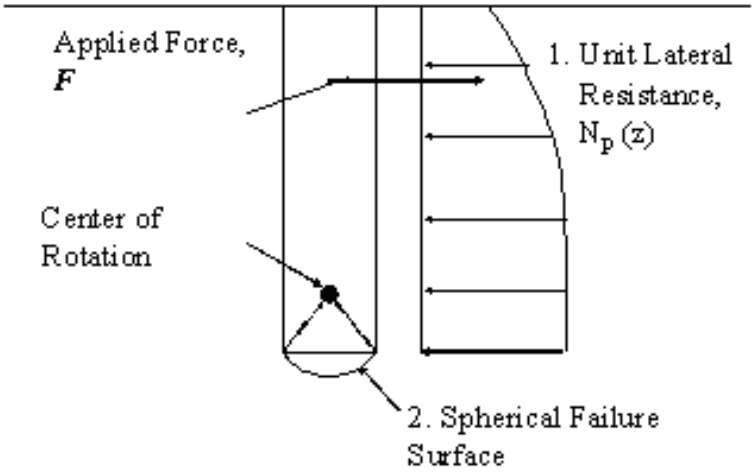

Figure 2. Simplified Analysis by Aubeny et al. (2001)

process of seeking a least upper bound. The simplified framework presented above permits solution in a spreadsheet format.

Parametric Studies

Using the simplified analyses, the PI's investigated the influence of a number of parameters on lateral load capacity of suction anchors, including anchor-line attachment depth, caisson aspect ratio, soil strength profile characteristics, adhesion conditions at the soil-caisson interface, and the possible occurrence of a gap at the soil-caisson interface on the windward side of the caisson. A comprehensive parametric study is given by Aubeny et al. (2001). It should be noted that a model based on mechanics principles such as this allows such studies, whereas empirical models do not.

An example of the computer program's capabilities is given in Figure 3. The analysis considers the hypothetical case of a 60-ft long by 15-ft diameter caisson in a soil having an undrained shear strength of 50 lb/ft^2 at the mudline and increasing at a rate of 10 lb/ft^2 at per foot of depth. The analyses illustrate the importance of load attachment depth, with the lateral load capacity at the optimal attachment depth exceeding that at the mudline by a factor of about 4. In this case the optimal attachment depth is at about three-fourths of the caisson depth. The adhesion condition at the soil-caisson interface is of moderate significance, with the load capacity for a rough interface exceeding that for a smooth interface by up to 25%.

Suction Caissons under Inclined Loading

Using an approach originally proposed by Randolph (2001), the simple model of a rotating pile or caisson can be extended to conditions of inclined loading as shown in Figure 4. If v_0 is the lateral virtual velocity at the mudline, the axial velocity of the anchor, v_a, can be expressed as a ratio of this virtual velocity $v_a = \xi\, v_0$, where ξ is an optimization parameter. As described earlier for laterally loaded anchors, the lateral velocity at any point on the side of the caisson can be expressed in terms of the virtual velocity at the mudline, v_0, and the optimization parameter, L_0. Hence, the problem of inclined load capacity of a suction anchor can be formulated in terms of two optimization parameters, the depth to the center of rotation, L_0, and the ratio of vertical to lateral velocity at the mudline, ξ. While the additional optimization parameter increases the

complexity of the analysis somewhat, the computations are still well within the capabilities of spreadsheet calculations on a personal computer; therefore, the formulation described herein can be used as a practical design tool. Details of the formulation are given by Aubeny et al. (2003a) and Aubeny and Murff (2003). Key steps in the formulation are summarized below.

Side Resistance Interactions

A key component of the formulation for inclined loading involves the interactions between lateral and axial soil resistance acting on the sides of the caisson, resistance which is conveniently characterized by lateral and axial dimensionless bearing factors, N_{ps} and N_{ps}, respectively. The interaction between these bearing factors was evaluated through finite element analyses of a suction anchor, for which collapse loads were determined for various directions of translation ranging from purely horizontal to purely vertical. The shape of the interaction diagram is a function of depth. Figure 5

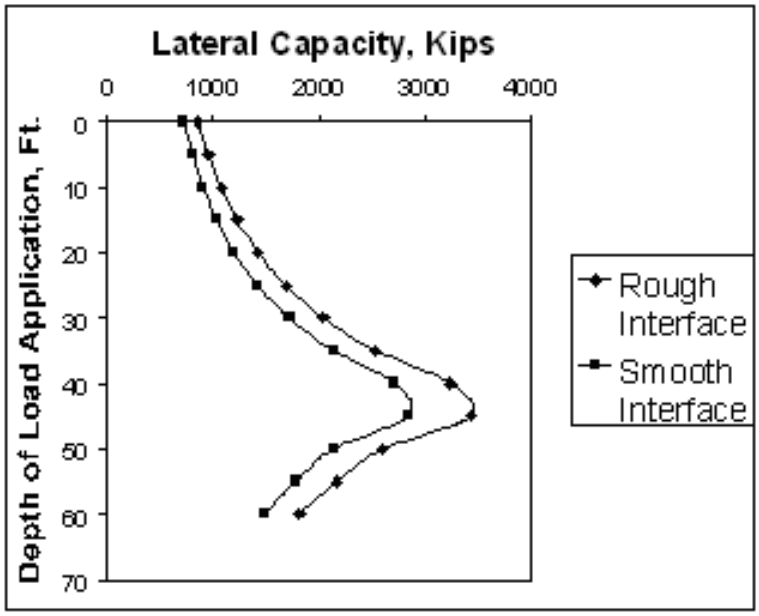

Lateral Capacity of a Suction Caisson vs. Depth of Load Application

(L=60 ft., D= 15 ft., s_{u0}= 50 psf, s_{u1}= 10psf/ft.)

Figure 3. Example of Simplified Analysis of Laterally Loaded Caisson

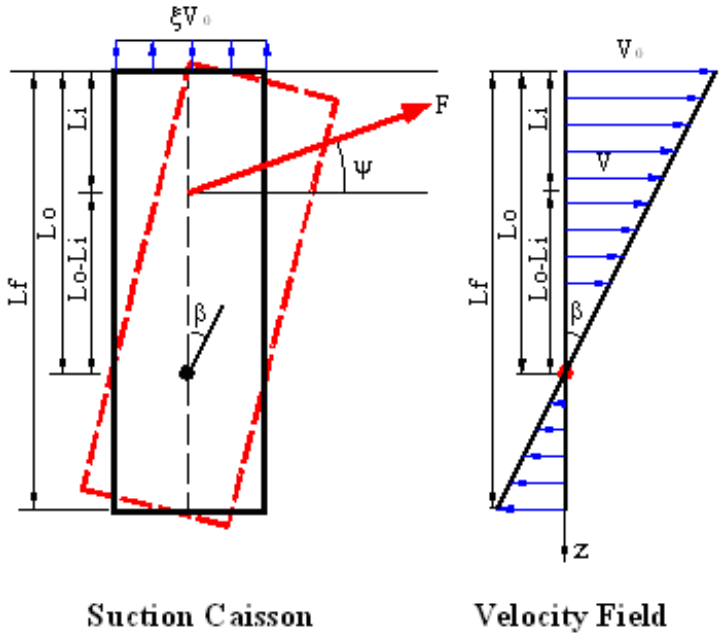

Figure 4. Deformation Mode for Caisson Subjected to Inclined Loading

shows an example interaction diagram corresponding to a point on the caisson corresponding to "deep" conditions; i.e. sufficient far from the mudline for free surface effects to be negligible.

Tip Resistance Interactions

Resistance at the tip of the caisson is comprised of vertical, horizontal, and moment resistance components. Based on a "scoop" mechanism, Bransby and Randolph (1998) proposed a relationship for "skirted" foundations subject to uplift loads that characterizes the interaction between all components of resistance. In this research, Aubeny et al. (2003a) proposed the simpler "circular" interaction relationship illustrated in Figure 6. Note that the terms V_0 and M_0 in Figure 6 denote the maximum vertical load capacity and moment resistance for conditions of pure vertical loading and pure rotation, respectively.

The Upper Bound Plasticity Framework

In the upper bound calculation discussed herein, the interaction diagrams in Figures 5 and 6 play a role directly analogous to that of the yield surface in classical plasticity theory. As an example, a determination of the internal energy dissipation due to soil resistance on the sides of the caisson would proceed according to the following steps:

For a given pair of optimization parameters L_0 and ξ (Figure 4), kinematic considerations fully define the axial and lateral components of velocity at any depth z on the side of the caisson, v_a and v_l.

The associated flow law dictates that the velocity vector (v_a, v_l) be normal to the interaction diagram in Figure 5. The point on the diagram at which this condition is satisfied, establishes the appropriate bearing factors N_{as}, N_{ps} at any depth z.

These bearing factors are applied to the following expression for

$$\dot{D}_s = \int (\alpha N_{as} S_u D v_a + N_{ps} S_u D v_l) dz \qquad \text{(Eq. 1)}$$

where $\dot{D}_s$ is internal energy dissipation, α is an adhesion factor at the soil-caisson interface, S_u is local soil undrained shear strength, and D is caisson diameter.

Calculations for vertical and moment resistance at the caisson tip using Figure 6 follow an identical sequence.

Parametric Studies

Examples of suction caisson load capacity interaction diagrams for a caisson with aspect ratios L_f/D = 2, 6, and 10 in a uniform strength profile are given in Figure 7. In these examples, the caisson is rough (adhesion factor α = 1) and no gap is assumed on the windward side of the caisson. Aubeny et al. (2003a) give a comprehensive parametric study of inclined load capacity of suction caissons based on this procedure. Interaction diagrams have been developed for other conditions including non-uniform strength profiles (Aubeny et al., 2003a) and adhesion factors α less than unity (Aubeny et al., 2003b).

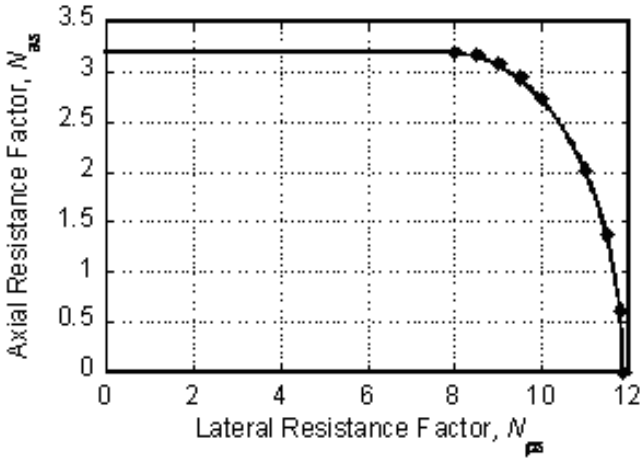

Axial-Lateral Resistance - Interaction Diagram

Figure 5. Axial-Lateral Caisson Side Resistance Interaction for 'Deep' Conditions

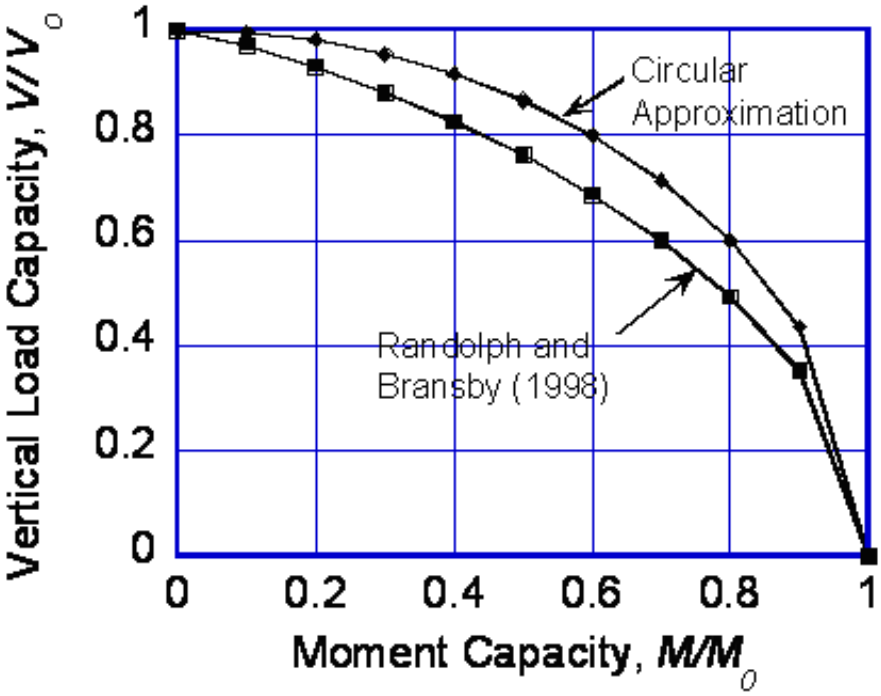

Figure 6. Axial-Rotational Caisson Tip Resistance Interaction

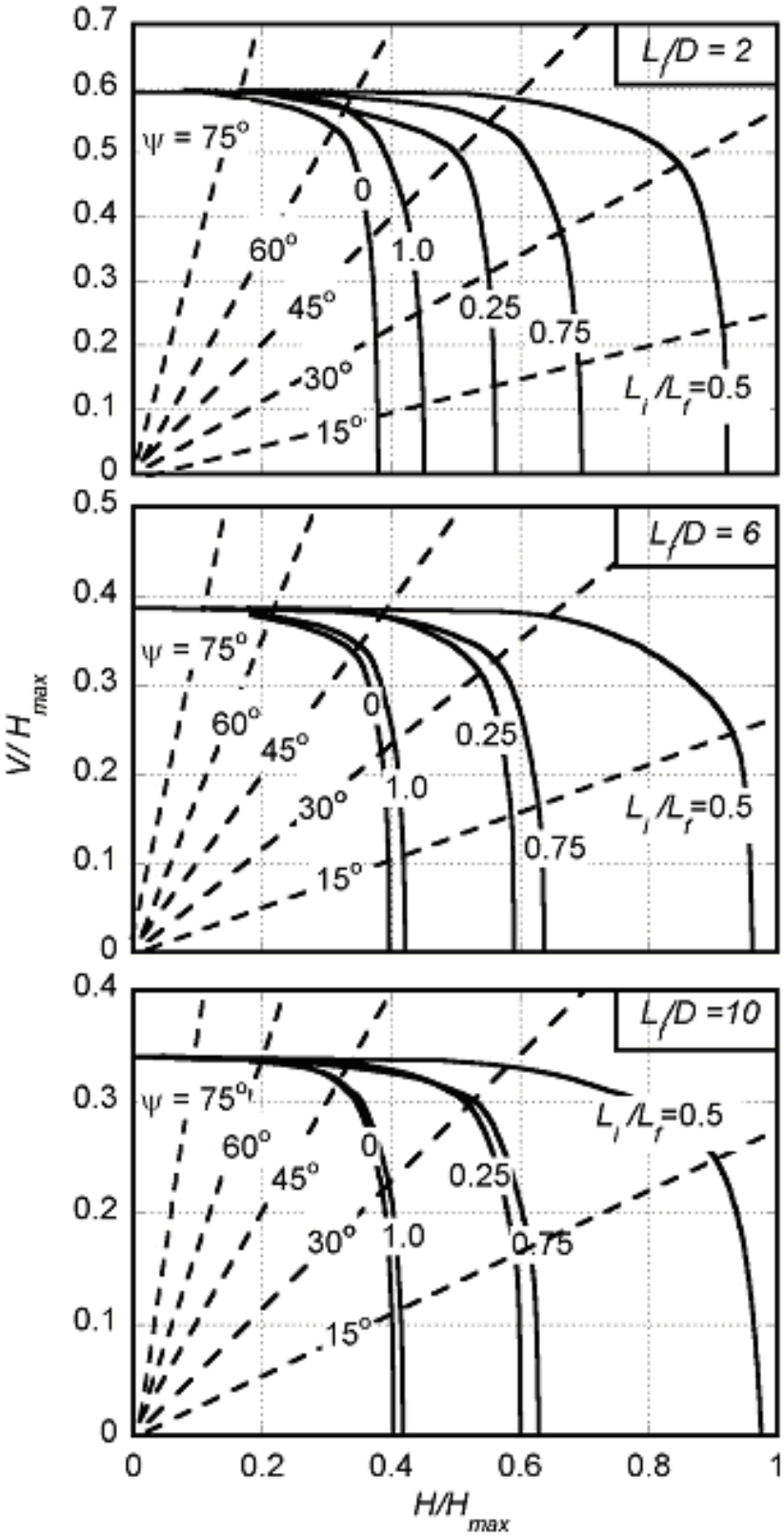

Figure 7. Caisson Inclined Load Capacity in Uniform Soil Strength Profile

Influence of Soil Strength Anisotropy

The suction anchor load capacity predictions presented above assume isotropic strength properties for the clay. In actuality, the anisotropic strength properties of clays are well-established. A study was therefore directed toward investigating the effects of strength anisotropy on suction anchor load capacity predictions.

Clay Strength Anisotropy

The studies focused on K_0 consolidation conditions. In this case, the relevant shearing conditions become triaxial compression, triaxial extension, simple shear, and pressuremeter (cavity expansion) shear. The undrained simple shear strength S_{uDSS} typically represents an "average" of triaxial compression and extension conditions. Hence, S_{uDSS} is typically considered the most appropriate strength measure to use in an isotropic analysis, and it provides a useful reference measure for assessing the effects of anisotropy. Data by Ladd (1991) show the strength in triaxial compression to exceed that in simple shear by a factor S_{uTC}/S_{uDSS} =1.04-1.56, while typical data for triaxial extension indicate a range S_{uTE}/S_{uDSS} = 0.55-0.96. Limited test data on the pressuremeter shearing mode (Wood, 1981; O'Neill, 1985; Whittle and Aubeny, 1993) suggest S_{uPM}/S_{uDSS} =1.

Anisotropic Plasticity Model

To simulate the behavior described above, this research adopted an anisotropy model proposed by Hill (1950), which was modified to specify different yield surfaces for triaxial compression and extension. Figure 8 contrasts the modified Hill model to the von Mises model used in the isotropic analyses. Also shown is an elliptical yield surface originally proposed by Davis and Christian (1971).

The modified Hill yield model was incorporated into the original Murff and Hamilton (1993) three-dimensional model for a laterally loaded pile. Derivation of the internal energy dissipation relationships for continuously deforming regions followed the approach presented by Murff (1978). The Murff-Hamilton pile failure mechanism also contains discrete slip planes. This research developed expressions for internal energy dissipation along a slip plane in an anisotropic material by modifying expressions developed earlier by Murff (1980) applicable to isotropic materials.

Parametric Studies

To assess the effects of anisotropy on suction anchor lateral load capacity, plastic limit analysis predictions were made for the 4 cases of anisotropic undrained shear strength conditions listed in Table 1. It should be noted that for the von Mises (isotropic) yield condition, $S_{uTC}/S_{uDSS} = S_{uTE}/S_{uDSS} = 0.87$. Predictions were made with and without a gap being assumed to form at the soil-caisson interface on the windward side of the anchor.

Table 1. Strength Parameters Considered in Parametric Study

Case	S_{uTC}/S_{uDSS}	S_{uTE}/S_{uDSS}
A	1.33	0.96
B	1.33	0.55
C	1.04	0.96
D	1.04	0.55

Figure 9 indicates that the isotropic load capacity predictions deviate from the more rigorous anisotropic predictions by no more than 10%. For conditions of no gap formation, anisotropy effects were most significant for short, squat caissons, having aspect ratios less than 6. When a gap forms on the windward side of the caisson, anisotropy affects load capacity at all anchor aspect ratios, but the anisotropic analysis predictions still deviate from the isotropic analyses by no more than 10%. Overall, it was concluded from this study that the effect of strength anisotropy on suction anchor capacity is relatively modest. However, the database on undrained strength anisotropy is relatively limited, and anisotropic conditions outside the range of that considered in the study may well be possible. Hence, the potential influence of strength anisotropy should not be entirely discounted. Full details of the anisotropy study, including comparisons to finite element studies, are documented by Aubeny et al. (2003c).

Model Evaluation

Plastic limit analysis predictions of suction anchor load capacity have be validated at TAMU through comparisons to centrifuge model tests (Clukey et al., 2003) and finite element analyses (Anderson et al., 2003). Single gravity model tests of suction anchors subjected to general loading have also been performed at the University of Texas (UT).

Preliminary evaluation of the UT data indicates favorable comparison to the OTRC plasticity model predictions (Rauch, 2003).

Centrifuge Test Data

Centrifuge model tests performed at the C-CORE testing facility (Clukey and Phillips, 2002) were compared to load capacity predictions from the TAMU plasticity model in a study documented by Clukey et al. (2003). Seven centrifuge tests were performed in soil conditions approximating normal consolidation for load inclination angles ranging from 24 to 90 degrees from horizontal. The soil strength profiles in the centrifuge tests were estimated from (1) piezocone tests, and (2) simple shear tests used in conjunction with the SHANSEP normalization procedure. Plastic limit analyses were performed using the best estimate of the soil strength profiles to obtain anchor load capacity predictions corresponding to the conditions of the centrifuge tests. The caisson anchors used in the tests had aspect ratios (depth/diameter) in the range 4.7-4.9, with the pad-eye located at about two-thirds of the caisson depth. Direct measurements of the soil-caisson adhesion factor were not made for these particular tests; however, based on experience, a range $\alpha = 0.7$ to 1.0 was considered.

Figure 10 shows the comparisons between analyses and measurements. Overall, the agreement was considered quite good considering the uncertainties in the soil strength profile. Particularly noteworthy was the agreement between model and measurement with regard to the load inclination angle at which interaction effects develop; i.e., the region in which the vertical-horizontal load capacity diagram is curved. Figure 10 shows that both theory and measurement show that interaction effects occur for load attachment angles less than 40-45 degrees from horizontal. It should be noted that the interaction relationship between vertical and horizontal load capacity shown in Figure 10 is unique to the particular conditions of the tests. The plasticity model predictions (Figure 7) indicate that the characteristics of the interaction diagram are sensitive to both caisson aspect ratio and load attachment depth.

Finite Element Analyses

A comprehensive study on deepwater anchors by Anderson et al. (2004) included comparisons between simplified analysis methods and more rigorous finite element

predictions of suction anchor load capacity. The study considered short (L_f/D = 1.5) and slender (L_f/D = 5) caissons in normally and lightly over-consolidated soil profiles. The four hypothetical cases are shown in Table 2.

The study by Anderson et al. (2004) first established benchmark solutions based on finite element studies from three organizations: Norwegian Geotechnical Institute (NGI), the Center for Offshore Foundation Systems (COFS) at the University of Western Australia, and the Offshore Technology Research Center (OTRC). The benchmark solutions were used to evaluate four simplified prediction methods: P1 (OTRC), P2 (COFS), P3 (NGI), and P4 (an industry predictor). The OTRC predictions utilized the simplified plastic limit analysis procedure for inclined loading conditions described earlier. Simplified solutions were compared to finite element solutions with regard to (1) anchor vertical holding capacity, (2) anchor horizontal capacity, (3) anchor capacity at intermediate load inclination angles, (4) optimal load attachment depth corresponding to maximum horizontal holding capacity, (5) load capacity for an anchor line attachment depth greater than optimum, and (6) load capacity for an anchor line attachment depth less than optimum.

The ratios of simplified analysis to finite element predictions are presented in Table 3. In all cases, the P1 (OTRC) simplified method predictions are always within 20% of the FEM benchmark values, and in most cases they are within 10%. Some of the larger differences between simplified and benchmark solutions were associated with vertical holding capacity estimates. This may be due in part to the idealized failure mechanism assumed in the development of this method, in which vertical side resistance and tip resistance are considered as two distinct, independent mechanisms. In actuality, some interaction occurs between these mechanisms, an effect that can be captured in finite element analyses but not in the simplified plasticity formulation.

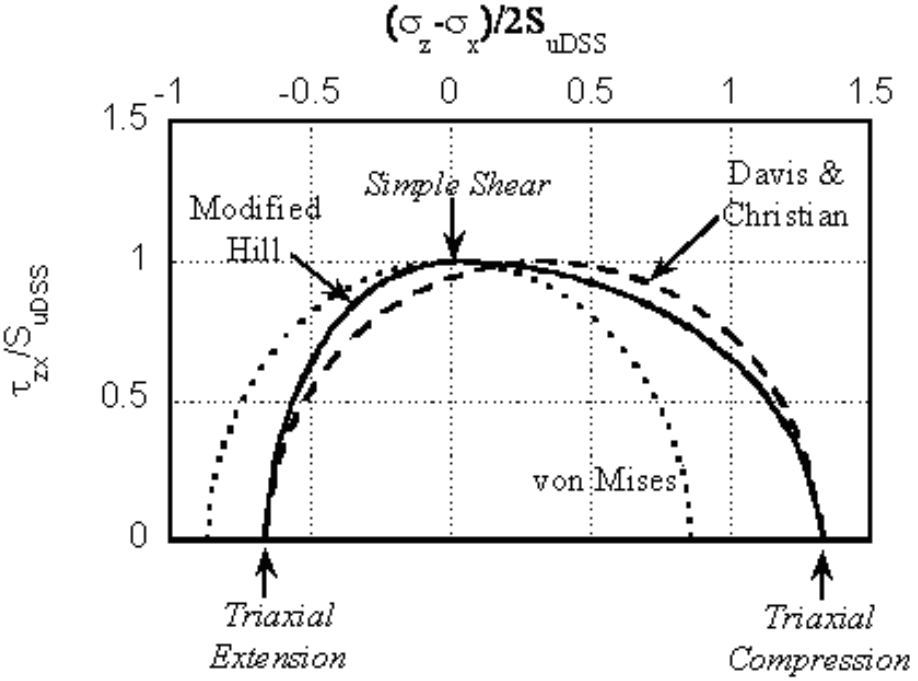

Figure 8. Anisotropic Yield Surfaces

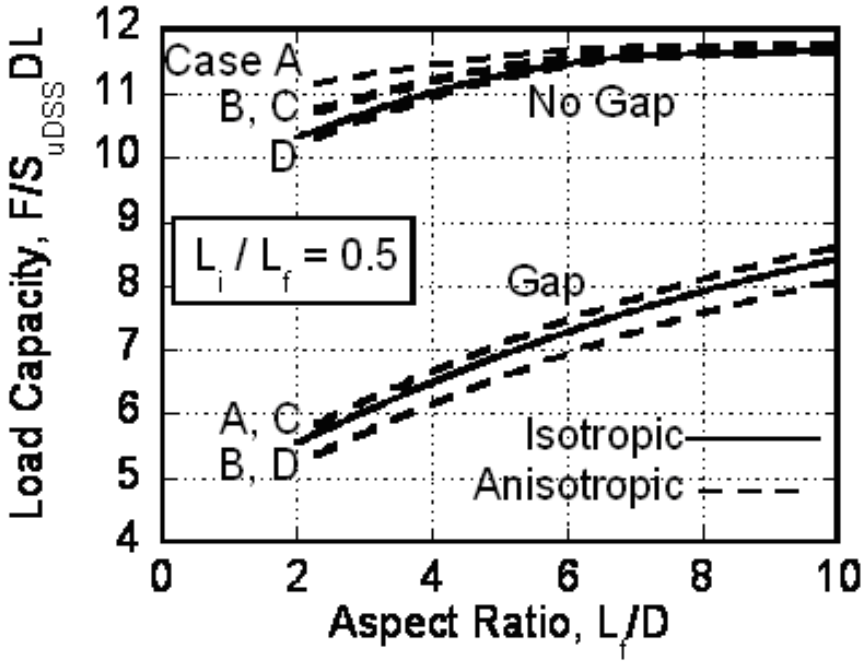

Figure 9. Influence of Strength Anisotropy on Predicted Suction Anchor Capacity

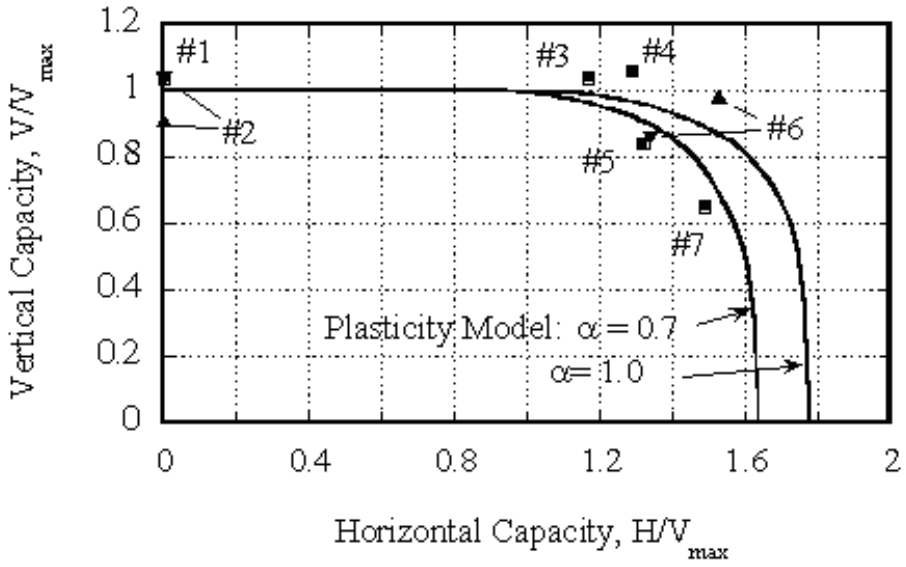

Figure 10. Load Capacity of Suction Anchors - Comparison of PLA Model Predictions to Centrifuge Test Results

Table 2. Geometry and Soil Profile Data for Studies Comparing Simplified Methods of Analysis to Finite Element Predictions (after Anderson et al., 2004).

Case	C1	C2	C3	C4
Geometry				
Outside Diameter	5m	5m	5m	5m
Target penetration depth	25m	7.5m	25m	7.5m
Depth/Diameter ratio	5	1.5	5	1.5
Structural model	Rigid cylinder with closed top			
Submerged weight	1100kN	330kN	1100kN	330kN
Soil data				
Overconsolidation ratio	1		~1.6	
S_{uDSS}	1.25z (kPa)		10kPa for z<5m 2z (kPa) for z>5m	
S_{uTC}	1.2 S_{uDSS}			
S_{uTE}	0.8 S_{uDSS}			
S_u vertical plane	S_{uDSS}			
Shear strength along outside skirt wall	0.65 S_{uDSS}			
σ'_{vc}	6z (kPa)		7.2z (kPa)	
K_0	0.55		1.0 (z<5m) 0.65 (z>5m)	

Table 3. Ratio between capacity calculated by simplified methods and 3D finite element analyses (after Anderson et al., 2004).

CASE	Predictor	C1	C2	C3 no crack	C3 with crack	C4 no crack	C4 with crack
Anchor Lf/D:		**5**	**1.5**	**5**	**5**	**1.5**	**1.5**
OCR:		**1.0**	**1.0**	**~1.6**	**~1.6**	**~1.6**	**~1.6**
Vertical capacity	P1	0.98	0.83	0.98	1.20	0.86	0.99
	P2	0.88	0.85	0.87	0.85	0.88	0.90
	P3	0.94	0.93	0.93	1.00	0.97	1.03
	P4	0.98	0.82	0.89	0.89	0.67	0.68
Horizontal capacity	P1	0.95	1.03	0.95	1.09	1.03	0.99
	P2	0.98	1.19	0.97	1.11	1.14	0.99
	P3	0.95	0.89	0.95	1.03	0.89	0.87
	P4	0.97	0.98	0.98	1.03	0.85	0.85
Capacity at intermediate load inclination, α	□	22.5/30o	45/60o	22.5/30o	22.5/30o	45/60o	45/60o
	P1	/0.97	1.01/0.98	/1.02	/1.18	1.01/0.89	1.06/1.06
	P2	/0.95	1.14/1.02	0.96/0.95	1.03/0.91	1.07/0.91	1.01/0.95
	P3	/0.97	0.91/1.00	0.97/1.00	1.05/0.95	0.98/0.98	0.96/1.03
	P4	/0.88	1.01/0.94	0.98/0.98	1.03/0.85	0.77/0.69	0.84/0.72
Depth of optimum load attachment	P1	1.01	1.01	1.02	1.02	1.00	1.02
	P2	1.06	1.01	1.02	1.00	1.00	1.02
	P3	1.01	1.01	1.02	1.00	1.00	1.00
	P4	1.03	1.03	1.02	1.00	1.08	1.05
Attachment point below optimum	P1	0.95	1.00	0.93	(1.09)	0.96	0.89
	P2	0.91	1.33	0.99	(1.09)	1.06	1.13
	P3	0.98	1.00	1.00	(1.20)	0.95	1.04
	P4	0.99	1.55	1.16	(1.00)	1.48	1.38
Attachment point above optimum	P1	1.04	0.92	1.10	1.18	0.96	0.99
	P2	1.06	1.10	1.08	1.01	1.14	0.99
	P3	0.90	0.95	0.98	0.91	0.92	1.01
	P4	0.78	0.89	1.03	1.05	0.75	0.80

Note: Predictor P1 = OTRC method.

Shading indicates the following:

Difference ≤ 10%	
Difference 10 to 20%	
Difference >20%	

PROGRESS AND RESULTS – VERTICALLY LOADED ANCHORS

Prediction of the holding capacity of vertically loaded anchors (VLA's) involves solving two major problems: (1) prediction of the trajectory of the anchor during drag embedment, and (2) estimation of the pullout capacity corresponding to the estimated embedment depth. The problems are actually somewhat inter-related, since prediction of the anchor trajectory requires a succession of estimates of collapse loads of the embedded anchor at various instants of time throughout the drag embedment process. The methodology for estimating the instantaneous collapse loads is essentially the same as that for estimating vertical pullout capacity, except that the re-positioning of the anchor must be taken into account for the vertical pullout capacity calculation. It should also be noted that the need for prediction of anchor trajectory during drag embedment is common to the drag embedment anchors (DEA's) used in conventional catenary mooring systems as well as VLA's. Hence, much of the analytical procedures and databases developed for DEA's are relevant to the VLA research effort.

Analytical Approach

As with suction anchors, this research employs a general upper bound plasticity approach to estimating anchor trajectory and capacity. Key elements of the formulation are presented below.

Soil Resistance on Rectangular Flukes

A first step in analysis of a penetrating anchor is characterizing the soil resistance acting on the anchor fluke and shank. For brevity, this report focuses on the fluke. Kim (2005) presents an analogous formulation for the shank. In developing a formulation for soil resistance, it is most convenient to describe fluke motions in terms of a tangential velocity v_s and a rigid body rotation about a center of rotation located on the *s*-axis in Figure 11. The direction normal to the long axis of the fluke is taken as the *p*-direction. The soil resistance force (per unit thickness into the page) parallel to the fluke F_s can be expressed in terms of soil undrained shear strength (S_u), fluke length (L_f), fluke thickness (w_f), and a soil-anchor adhesion factor (α):

$$F_s = 2\, S_u\, [\alpha\, L_f + N_{ps}\, w_f] \qquad \text{(Eq. 2)}$$

A reasonable estimate of the end bearing factor is N_{ps} =12.

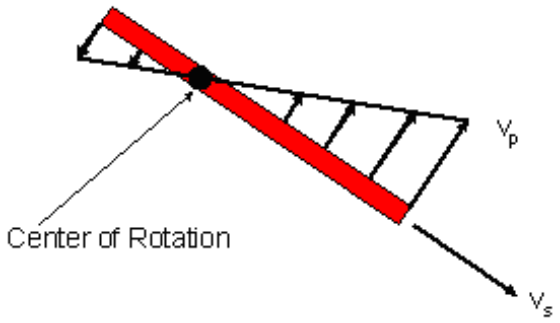

Anchor Kinematics

Figure 11. Kinematics of a Penetrating Anchor Fluke.

Soil resistance normal to the fluke is modeled as a uniform pressure (Figure 12) that is proportional to soil strength:

$$q = n_p S_u \qquad \text{(Eq. 3)}$$

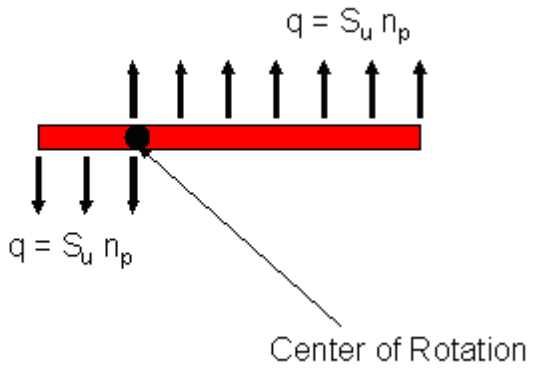

Figure 12. Soil Resistance to Fluke Rotation

Solutions from plasticity theory indicate that the appropriate average bearing factor for rotation about the center of the plate is $n_p = 6$, while for rotation about the edge of the plate $n_p = 12$. As a trial solution for intermediate conditions of rotation, n_p is assumed to vary as a second order function of distance of the center of rotation to the center of the fluke:

$$n_p = 6 + 6\, d_c^2 / (L/2)^2 \qquad \text{(Eq. 3)}$$

where d_c is the distance from the center of the fluke to the center of rotation, and L is the length of the fluke. A check on whether the above assumptions are reasonable is possible by considering resistance functions for the entire fluke:

$$V = N_p\, S_u\, L \qquad \text{(Eq. 4)}$$

$$M = N_m\, S_u\, L^2 / 4 \qquad \text{(Eq. 5)}$$

where V is the total soil resisting force acting normal to the long axis of the fluke, M is the soil resisting moment acting on the fluke, and N_p and N_m are dimensionless bearing factors. Figure 13 shows the interaction between N_p and N_m implied from Eq. 3. This interaction relationship is considered an acceptable solution in the sense that it is convex everywhere and satisfies the limiting conditions; i.e., for pure translation normal to the fluke N_p =12, and for pure rotation about the center of the fluke $N_p = 6$.

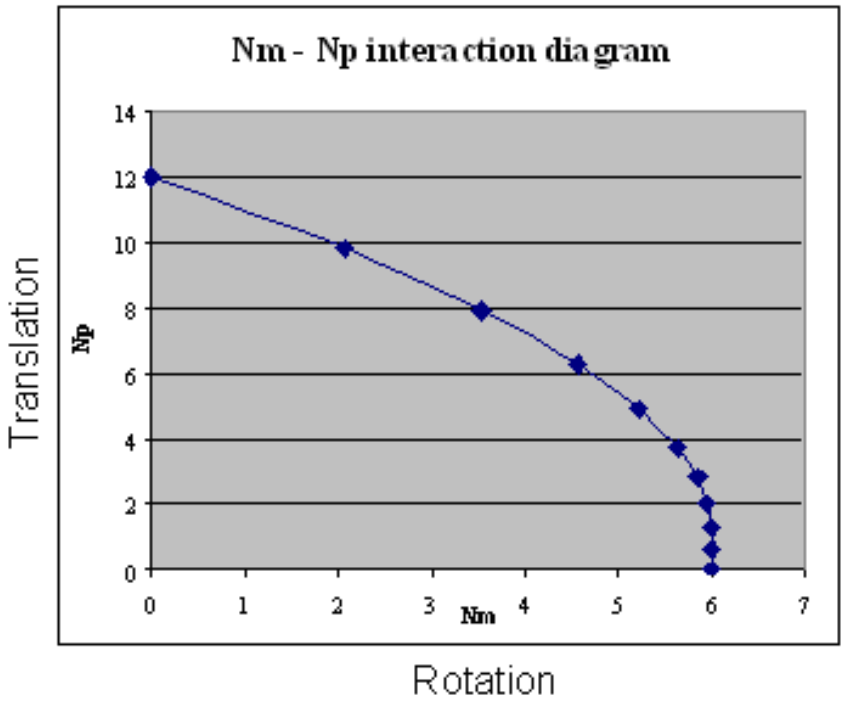

Figure 13. Interaction Diagram for Fluke Rotation-Translation

Soil Resistance for Non-Rectangular Flukes

The interaction relationships described above are expressed in terms of a parameter dc defining the distance between the center of rotation of the plate and a reference point. For the case of a rectangular plate in a soil having uniform strength, taking the center of the plate as a reference point produces reasonable results. However, many practical situations involve non-rectangular plates and/or non-uniform soil strength profiles. In these cases the most appropriate reference point for describing the center of rotation is far from obvious. Kim (2005) recommends a reference point at which the internal energy dissipation is a minimum when the fluke is rotated about that point. This approach appears to yield reasonable interaction diagrams (similar in form to Figure 13) even for complex plate geometries and soil conditions. Kim (2005) provides a detailed description and justification for this approach.

Upper Bound Analysis of Instantaneous Collapse Load

With soil resistance defined as described above, the total internal energy dissipation associated with the anchor motion is computed by multiplying particle velocity of a point on the plate (Figure 11) by soil resisting stress (Eqs. 2 and 3) and integrating over the area of the plate. By equating internal energy dissipation to external work performed by the anchor line at the shackle, a collapse load F is computed. Detailed equations describing the formulation are given by Kim (2005). This collapse load corresponds to an arbitrarily assumed center of rotation of the anchor. The procedure is systematically repeated for a series of centers of rotation to obtain a minimum collapse load F_{min} that is taken as the solution. Since the collapse load corresponds to a kinematically admissible motion of the anchor, it constitutes an upper bound solution, with F_{min} taken as a least upper bound solution. Figure 14 illustrates the procedure. The contours in this figure represent collapse load F corresponding to various centers of rotation (x_0, y_0). Note that the solution provides information on both the minimum collapse load F_{min} as well as the kinematics (center of rotation) of the anchor.

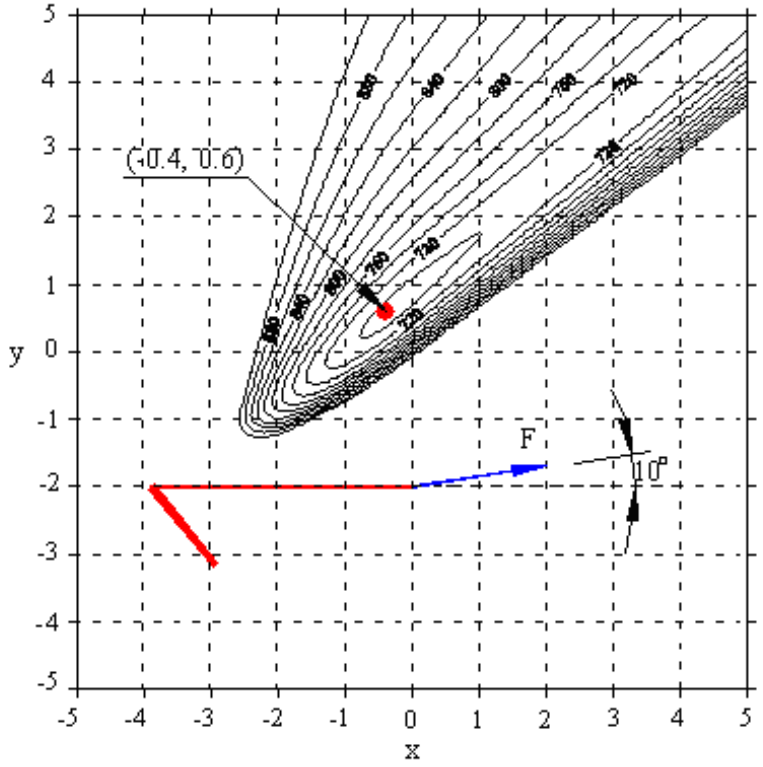

Figure 14. Contours of Anchor Resultant Force for 10o Force Inclination Angle

Characteristic Curve

The analysis outlined in the preceding section is valid only for a prescribed angle of force inclination, 10^o in the case of the example shown in Figure 14. This procedure can be repeated for a full sweep of inclination angles. The result is illustrated in Figure 15. The computed locus of collapse loads F_{min} expressed as a function of force inclination angle θ_f is referred to as the characteristic curve for the anchor.

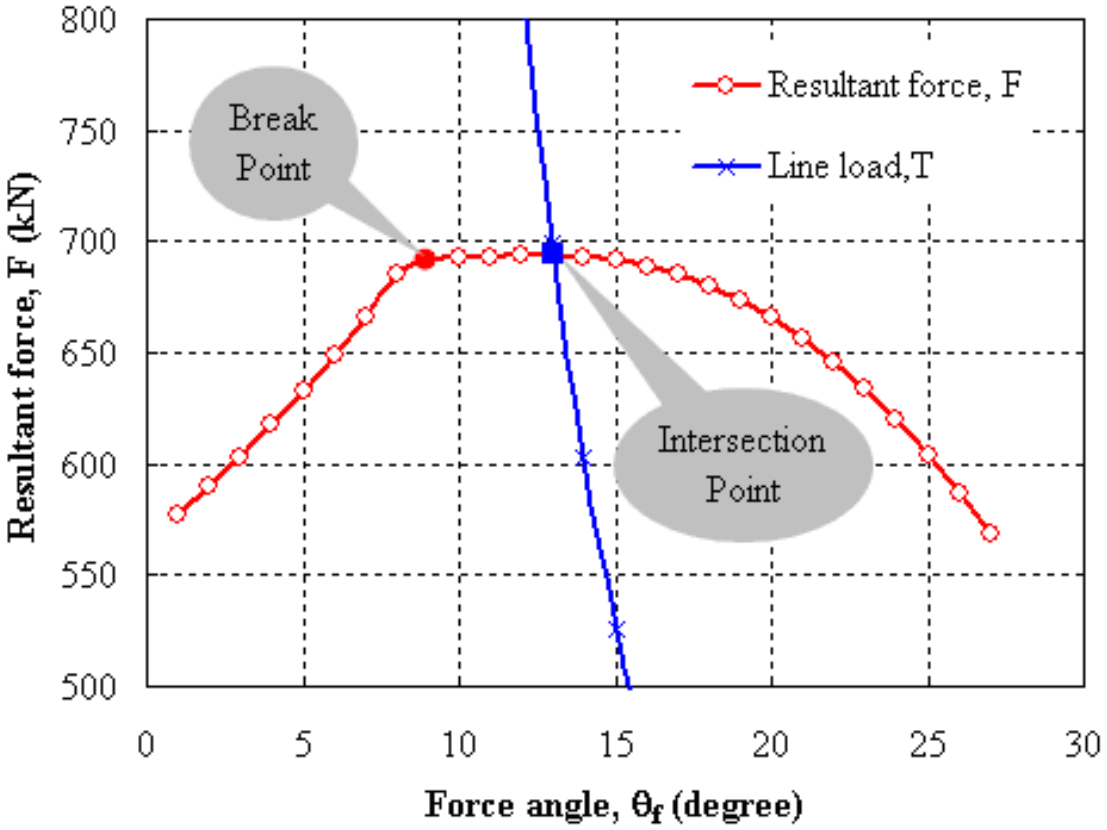

Figure 15. Example Characteristic Curve for Plate Anchor

The characteristic curve shows three distinct segments. The steeply rising portion of the curve at shallow force angles (up to about 9^o in example in Figure 15) corresponds to the anchor translating in the direction parallel to the fluke. At 9^o a break occurs in the characteristic curve. This break corresponds to a change in the anchor kinematics from translation parallel to the fluke to rotation, usually about a point close to the fluke. The second portion of the characteristic curve comprises a plateau extending from the break point. The characteristics of this plateau are governed by the properties of the shank;

indeed, for the case of an infinitely thin shank, the plateau is absent. The final segment of the characteristic curve steeply declines with increasing force angle.

An understanding of the characteristic curve is extremely important in understanding plate anchor behavior. The characteristic curve is influenced by fluke geometry, shank geometry, fluke-shank attachment point, and fluke-shank angle. Kim (2005) provides a detailed discussion of the effect of these factors on the characteristic curve.

Anchor Line Tension

The characteristic curve describes a locus of resultant anchor forces F_{min} corresponding to force inclination angles θ_f. The additional information required for a unique solution is provided by the relationship between anchor line tension versus anchor line angle at the shackle. For the case of a horizontal anchor line at the seabed, Neubecker and Randolph (1995) suggest the following equation:

$$\frac{T_a \theta_a^{\,2}}{2} = z_a \overline{Q} \qquad \text{(Eq. 6)}$$

In Eq. 6, T_a is anchor line tension, θ_a is the anchor line inclination angle at the shackle, z_a is the depth of the shackle, and $\overline{Q}$ is the average bearing resistance of the anchor line over the depth range z to z_a. Figure 15 shows Eq. 6 superimposed on the plot of an anchor characteristic curve. The intersection of the anchor line with the characteristic curve gives a unique solution for the magnitude and direction of the resultant anchor force.

Anchor Trajectory

The procedure described in the preceding sections allows one to compute the resultant anchor force magnitude and inclination at a given instant during the anchor penetration process. It also provides the coordinates of the center of anchor rotation at that instant of time. The final step in the anchor analysis is to incrementally advance the anchor to the next point in its trajectory. If the optimal center of rotation is located a finite distance from the fluke, then the anchor is in a rotational mode. In this case, the numerical algorithm rotates the anchor about this center at a fixed incremental angle, usually 1^o. If the optimal center of rotation occurs at a large distance from the anchor, the anchor is considered to be in a translational mode. In this case the numerical algorithm is advanced a fixed incremental vertical distance, usually 1 meter for a conventionally sized anchor.

In either case, after the anchor is advanced, the process described in the preceding sections for computing resultant anchor force is repeated for conditions at the new anchor depth and orientation. Successive repetition of this process produces an anchor trajectory curve. The process is continued until the anchor fluke is horizontal. Figures 16 and 17 show examples of predicted anchor trajectory and resultant force, respectively.

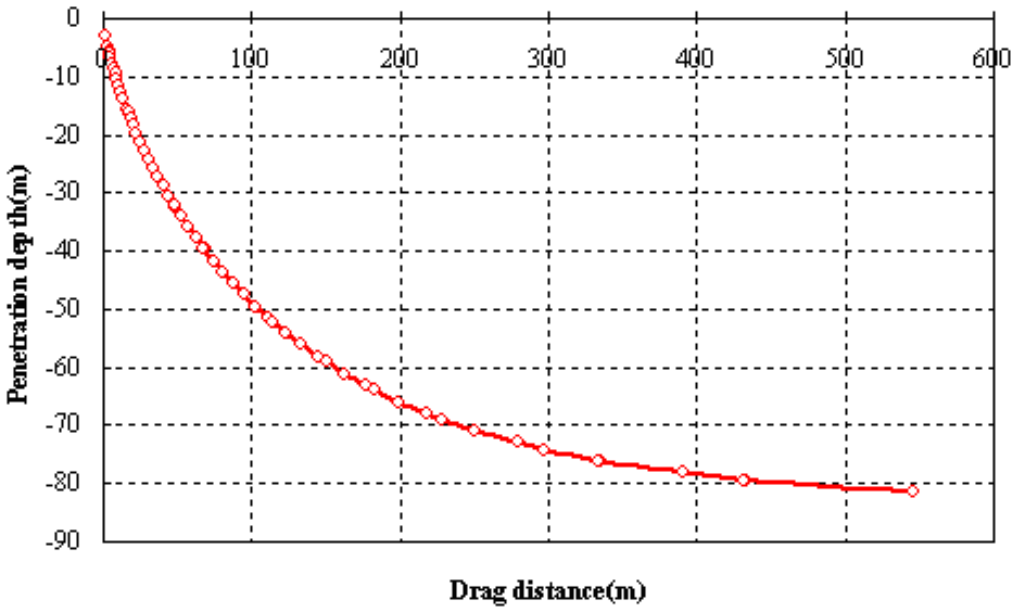

Figure 16. Anchor Trajectory for Example Simulation

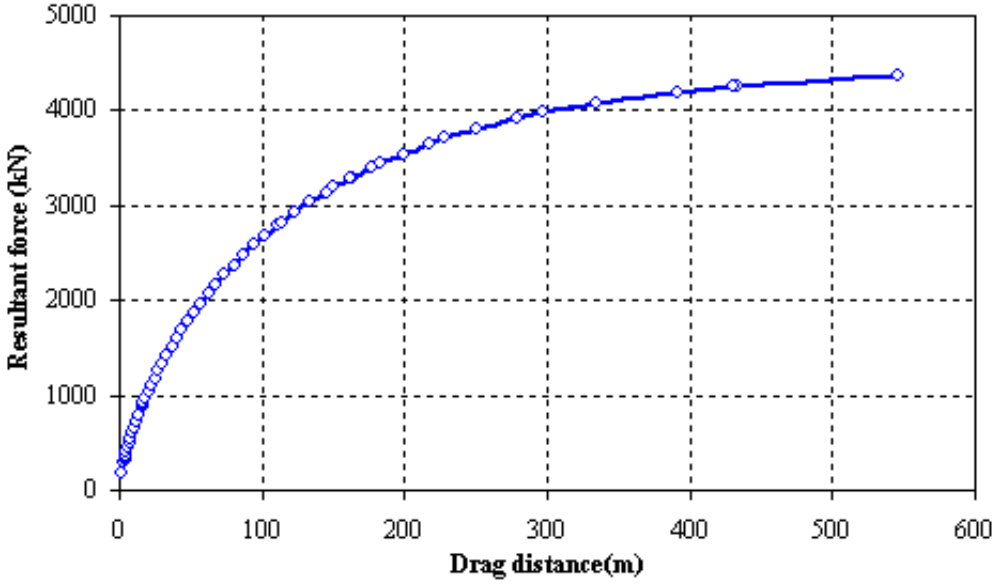

Figure 17. Resultant Anchor Force Example Simulation

The example simulation in Figures 16 and 17 involve a soil profile having a strength gradient of 1.5 kPa/m. The anchor has a 4-m long shank, a fluke-shank angle of 50^{o}, and a fluke-shank attachment point located at the trailing edge of the fluke. The fluke is rectangular with a length of 1.5 m and a width of 2 m into the page. Further details of the example simulation are given by Kim (2005).

Parametric Studies

One advantage of the model as formulated is that it lends itself well to performing parametric studies to assess the effects of anchor, soil, and anchor line characteristics. Kim (2005) performed a comprehensive series of studies investigating the influence of the variables outlined in Table 4.

Table 4. Summary of Model Parametric Studies by Kim

Element of Anchorage System	Factor Investigated
Fluke	Moment of Inertia Center of Gravity End Bearing Resistance Soil Sensitivity Weight of Fluke
Shank	Shape Length Fluke Shank Attachment Point Fluke-Shank Angle
Anchor Line	Line Diameter Line Bearing Resistance Soil Sensitivity Magnitude of Soil Strength Soil Strength Gradient

As is evident from Table 4, the parametric study was quite extensive, so this summary report will restrict its scope to the study of the effects of fluke moment of inertia. For a full presentation of the parametric study, the reader is referred to Kim (2005).

The fluke moment of inertia study considered the three flukes having equal areas but different moments of inertia (I) due to the differing shapes shown in Figure 18; i.e., rectangular, diamond, and butterfly. Taking the rectangular shape as a reference, it can be shown that:

$$I_{diamond} = 1/2 * I_{rectangular}$$

$$I_{butterfly} = 3/2 * I_{rectangular}$$

The moments of inertia in these cases are taken about the centroid of the areas.

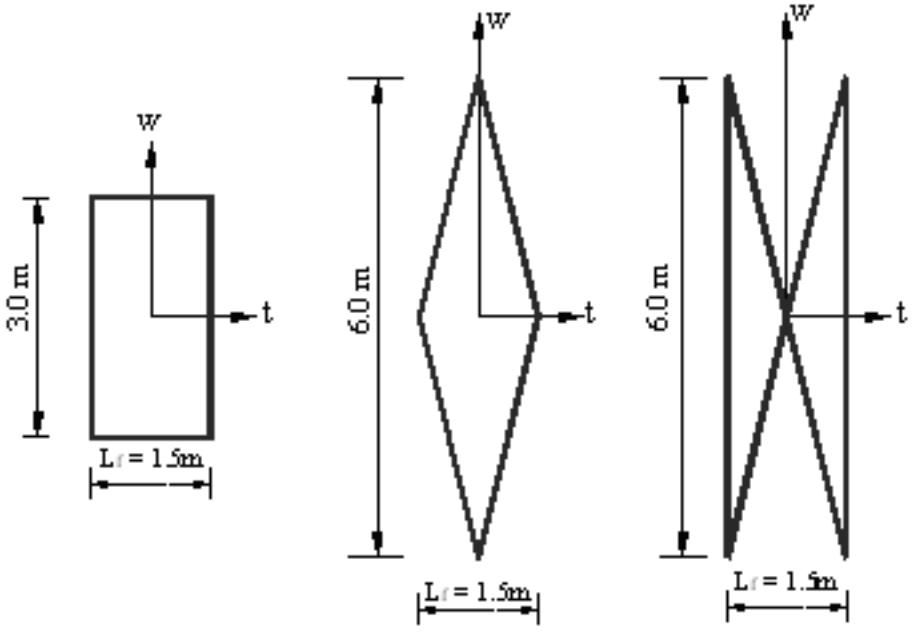

Figure 18. Fluke Configurations for Moment of Inertia Study.

Using the upper bound model for computing collapse loads presented in the previous sections, the characteristic curves for the three flukes have the shapes shown in Figure 19. A key aspect of the comparisons is that, with increasing moment of inertia, both the force angle and the resultant force at the break point increase. It should be recalled at this point that to the left of the break point the anchor moves in a translational mode, while to the right of the break point anchor rotation begins to occur. The implications on anchor capacity are twofold. First, the increased force angle at the break point means that the

anchor will tend to embed itself more deeply into the soil before the anchor begins to rotate and the trajectory flattens. Figure 20 illustrates this effect, where the butterfly anchor penetrates to the greatest depth while the diamond anchor penetrates the least. The second implication is that, since the resultant force at the break point largely controls anchor capacity, a larger moment of inertia leads to a greater anchor capacity. Figure 21, comparing the resultant forces for the three anchors, shows this effect. It should be noted that this particular parametric study was for the case of a uniform strength soil deposit. In the case of a soil deposit in which soil strength increases with depth, the greater penetration depth of the butterfly anchor will lead to further increase of anchor capacity due to the effect of the strength gradient.

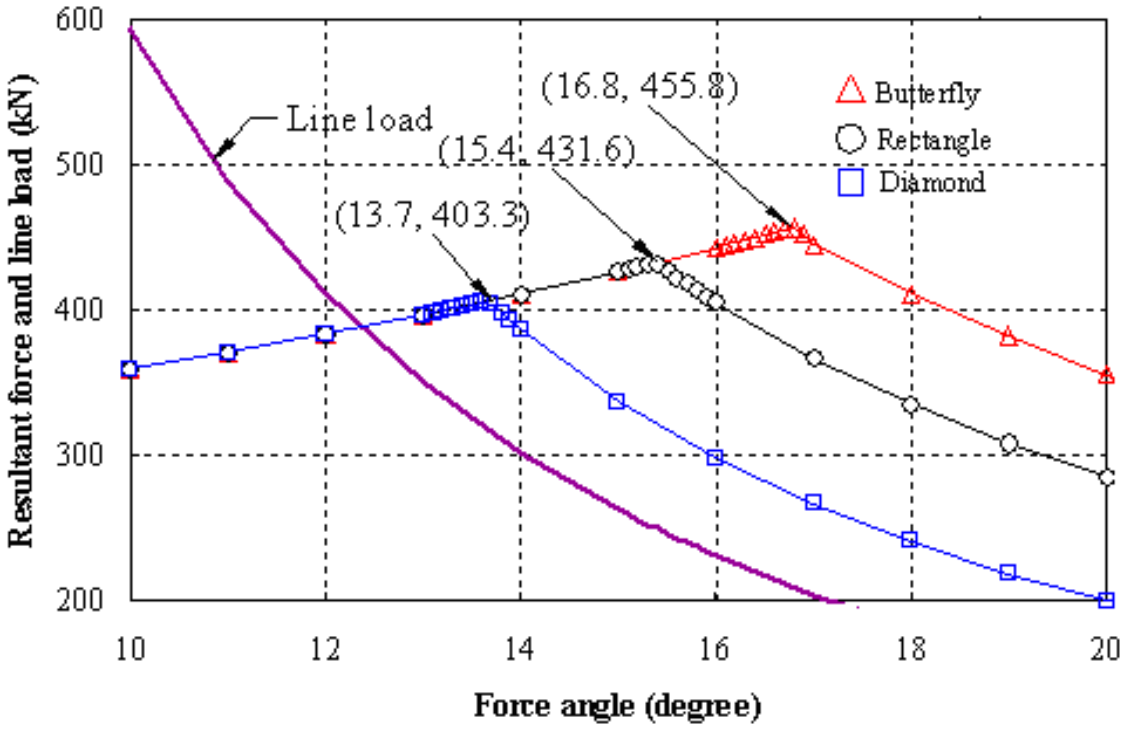

Figure 19. Anchor Characteristic Curves for Anchors Having Flukes with Equal Areas but Different Moments of Inertia

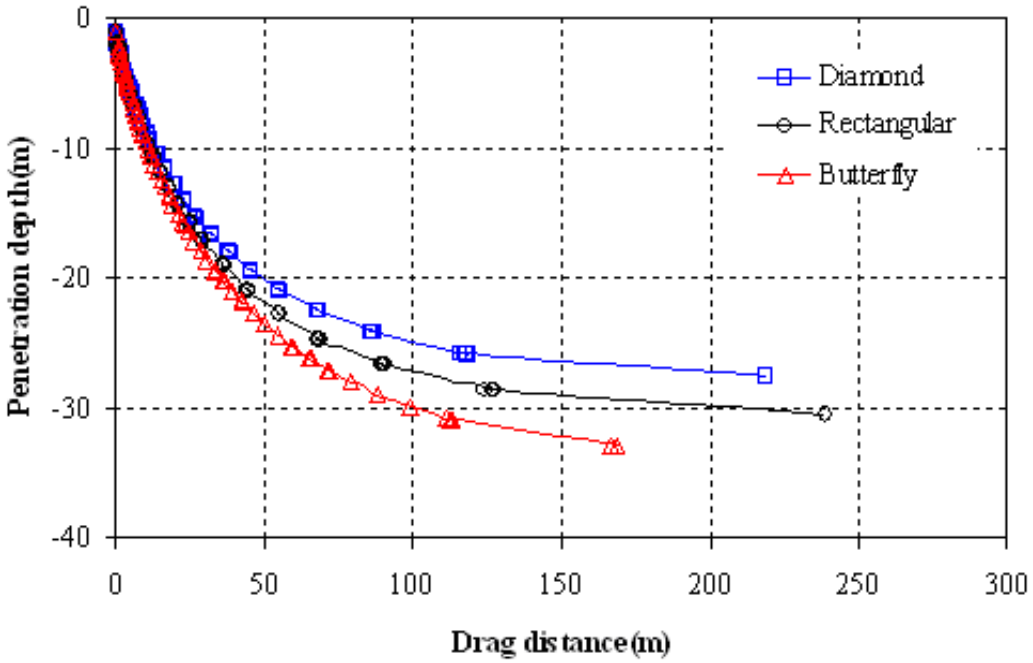

Figure 20. Trajectories for Anchors Having Flukes with Equal Areas but Different Moments of Inertia

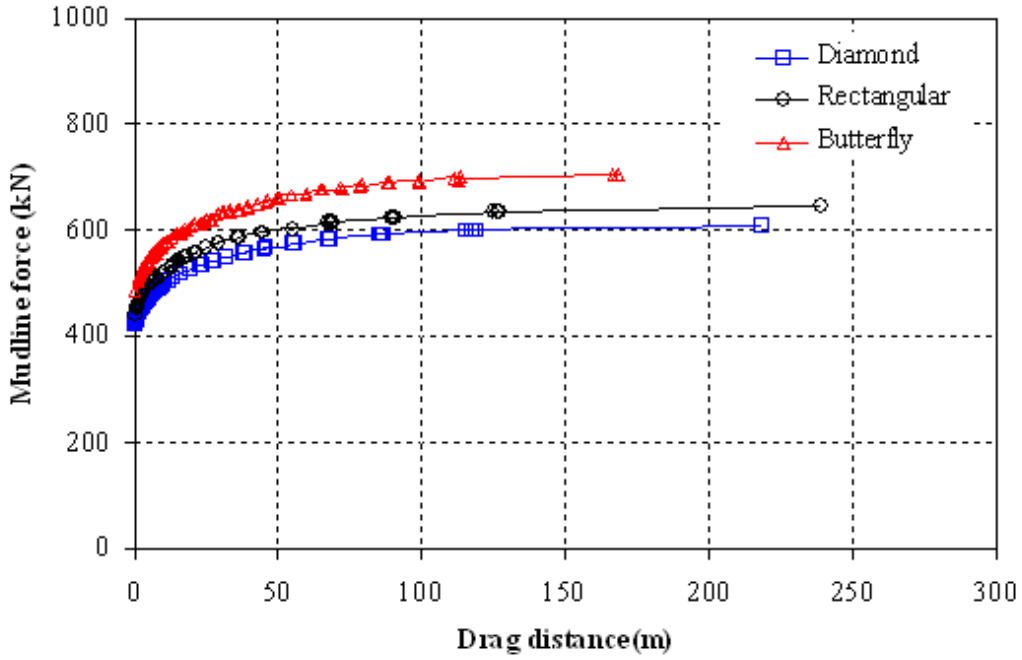

Figure 21. Mudline Forces for Anchors Having Flukes with Equal Areas but Different Moments of Inertia

Comparison to Measured Data

This research evaluated the upper bound model through comparisons to field tests, laboratory centrifuge tests, and existing empirical correlations. Table 5 lists the comparisons of field tests to predictions that were performed as part of this research. Kim (2005) gives a full presentation of these studies.

Table 5. Field Tests of Drag Embedment Anchors

No.	Project Name	Project Area	Year	Type of anchor
1	Joint Industry Project	Gulf of Mexico	1990	Vryhof Stevpris 68.6 kN
2	Liuhia 11-1 field	South China Sea	1996	Bruce FFTS MK4 392 kN
3	P-13 Site	Offshore Brazil	1997	Bruce Denla MK3 63.7 kN
4	South Timbalier Block 295	Gulf of Mexico	1996	Bruce Denla Mk2 12.74 kN
5	South Timbalier Block 295	Gulf of Mexico	1996	Vryhof Stevmanta 32 kN
6	Voador (P-27), Campos basin	Offshore Brazil	1998	Vryhof Stevmanta 102 kN

For this summary report, the 1990 Joint Industry Project (JIP) conducted in the Gulf of Mexico is used as an example for the comparative studies. The test under consideration involved a Stevpris 68.6 kN anchor in soft clay in a field installation designated as Test 7-4. Table 6 shows the anchor geometry and soil conditions assumed for the numerical upper bound analyses. The dimensions shown in Table 6 involved some idealization of the actual anchor geometry. Kim (2005) provides details of the actual versus simplified anchor geometry.

Figure 22 shows the measured versus predicted anchor trajectory, while Figure 23 shows measured versus predicted mudline forces during anchor installation. Both figures

indicate excellent agreement between analyses and measurement. It should be noted that, while the upper bound prediction of the trajectory in Figure 22 matches the measured trajectory up to a depth of about 21 meters, it predicts further possible anchor embedment down to a depth of about 29 meters. A plausible explanation for this mismatch is that the field test was terminated before the ultimate embedment depth was achieved. A similar explanation may apply to the mudline force predictions and measurements in Figure 23. The possibility that a field test was not necessarily conducted to the full embedment depth and capacity of the anchor should therefore be borne in mind when comparing field measurements to predictions.

Table 6. Anchor Geometry and Soil Condition for JIP Field Test

Property	Value
Anchor weight, W_a(kN)	68.6
Shank length, L_s(m)	4.485
Shank width, W_s(m)	3.93
Fluke length, L_f(m)	3.04
Fluke width, W_b(m)	Varied
Fluke depth, D_f(m)	0.2
Fluke-shank angle, (degree)	50
Anchor line diameter, b(m)	0.89
Surface undrained shear strength, S_{uo} (kPa)	0
Undrained shear strength gradient, S_{ug} (kPa/m)	1.57

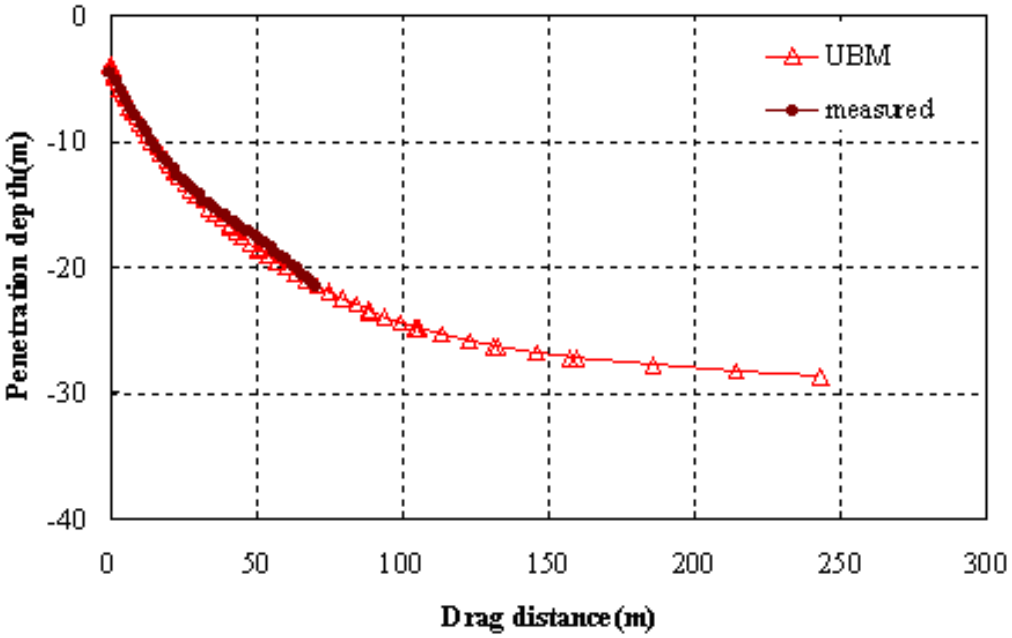

Figure 22. Predicted and Measured Relationship between Penetration Depth and Drag Distance for JIP Test 7-4.

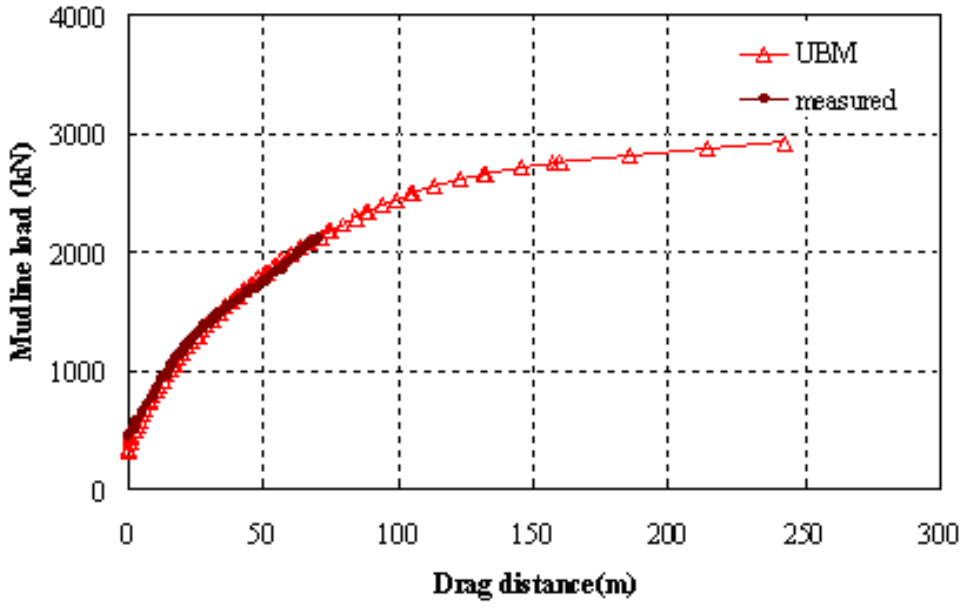

Figure 23. Predicted and Measured Relationship between Mudline Force and Drag Distance for JIP Test 7-4

CONCLUDING REMARKS

The models developed for the suction anchors and vertically loaded anchors are based on upper bound plastic limit analysis procedures. Since the analyses involves an optimization procedure for seeking a least upper bound, they may be considered less restrictive than alternative limit equilibrium analyses that require somewhat arbitrary assumptions with regard to the distribution of forces acting on the anchor. The algorithms developed in this research are spreadsheet based; hence, they provide analysis tools that are readily accessible to designers. A particular strength of these simplified analysis tools is that they can readily be utilized in parametric studies investigating the effects of a wide variety of soil conditions and anchor geometry on anchor performance. Validation studies to date indicate that the analysis procedures developed in this research can be used with confidence. Nevertheless, simplifying assumptions were made in developing the plastic limit analyses, so confirmation of final designs using more rigorous methods (e.g., finite element method) would be prudent, especially in cases involving unusual soil conditions or anchor geometry.

Suction anchor and VLA studies are considered largely completed. Remaining work in this area will involve publication of results in conferences and refereed forums.

REFERENCES

1. Andersen, K.H., Murff, J.D. Randolph, M.F., Clukey, E., Jostad, H.P., Hansen, B. Aubeny, C., Sharma, P., Erbich, C., and Supachawarote, C. (2005) "Suction anchors for deepwater applications," Keynote lecture International Symposium on Frontiers in Offshore Geotechnics, Perth, Australia, September 2005, pp. 3-30.
2. Anderson, K.H., Murff, J.D., and Randolph, M. (2004) Deepwater Anchor Design Practice, Final Year Report submitted to the American Petroleum Institute and the Deepstar JIP.
3. Aubeny, C.P, Kim, B.M, and Murff, J.D. (2005) "Proposed upper bound analysis for drag embedment anchors, International Symposium on Frontiers in Offshore Geotechnics, Perth, Australia, pp. 179-184.
4. Aubeny, C.P. and Murff, J.D. (2004) "Simplified limit solutions for undrained capacity of suction anchors," to be published in Journal of Ocean Engineering.
5. Aubeny, C.P., Han, S.W.*, and Murff, J.D. (2003a) "Inclined load capacity of suction caisson anchors," Intl. J. for Numerical and Analytical Methods in Geomechanics, Vol. 27, pp. 1235-1254.
6. Aubeny, C.P., Han, S.W. and Murff, J.D. (2003b) "Refined model for inclined load capacity of suction caissons," 22nd International Conference on Offshore and Arctic Engineering, June 8-13, Cancun, Mexico, OMAE2003-37502.

7. Aubeny C.P. Han S.W.*,and Murff, J.D. (2003c) "Suction caisson capacity in anisotropic soil," Intl. J. of Geomechanics, Vol. 3, No. 4, pp. 225-235.
8. Aubeny, C.P., Moon, S.K.*, and Murff, J.D. (2001) "Lateral undrained resistance of suction caisson anchors," Intl. J. Offshore and Polar Engineering, Volume 11, No. 3, pp. 211-219.
9. Clukey, E.C., Aubeny, C.P. and Murff, J.D. (2003) "Comparison of analytical and centrifuge model tests for suction caissons subjected to combined loads," 22nd International Conference on Offshore and Arctic Engineering, June 8-13, Cancun, Mexico, OMAE2003-37503.
10. Clukey, E. C. and Phillips, R. (2002) "Centrifuge Model Tests to Verify Suction Caisson Capacities for Taut and Semi-taut Legged Mooring Systems," Proceedings of the Deep Offshore Technology Conference, New Orleans.
11. Davis, E.H.and Christian, J.T. (1971) "Bearing capacity of anisotropic cohesive soil," ASCE J Soil Mech. and Found. Engr. Div, 97(SM5), pp. 753-769.
12. Hill, R. (1950) The Mathematical Theory of Plasticity, Oxford University Press, London.
13. Kim, B.Y. (2005) Upper Bound Analysis for Drag Anchors in Soft Clay, PhD Dissertation, Texas A&M University, College Station, Texas.
14. Ladd, C.C. (1991) "Stability evaluation during staged construction," ASCE J. Geotech. Engr,; 117 (4), pp. 537-615.
15. Matlock, H. (1970) "Correlations for design of laterally loaded piles in soft clay," Proc. 2nd Offshore Tech. Conf. Houston, pp. 577-594.
16. Murff, J.D., Randolph, M.F., Elkhatib, S., Kolk, H.J., Ruinen, R., Strom, P.J., and Thorne, C. (2005) "Vertically loaded plate anchors for deepwater applications," Keynote lecture International Symposium on Frontiers in Offshore Geotechnics, Perth, Australia, pp. 31-48.
17. Murff, J.D. (1980) "Vane shear testing of anisotropic, cohesive soils," Intl. Journal for Numerical and Analytical Methods in Geomechanics, 4, pp285-289.
18. Murff, J.D. (1978) "Upper bound analysis of incompressible, anisotropic media," Proc. 15th Annual Meeting of Engineering Science, pp. 521-526.
19. Murff J.D., and Hamilton J.M. (19930 "P-Ultimate for undrained analysis of laterally loaded piles," ASCE Journal of Geotechnical Engineering, 119 (1), pp. 91-107
20. Neubecker, S. R., and Randolph, M. F. (1995). "Profile and frictional capacity of embedded anchor chain", Journal of Geotechnical Engineering Division, ASCE, 121, 11, 787-803.
21. O'Neill, D.A. (1985) Undrained strength anisotropy of an overconsolidated thixotropic clay, MS Thesis, Dept. of Civ. And Envir. Engrg., MIT, Cambridge, Mass.
22. Prager, W. (1959) An Introduction to Theory of Plasticity. Addison Wesley, Reading, Massachusetts.
23. Randolph, M.F., and Houlsby, GT (1984) The limiting pressure on a circular pile loaded laterally in cohesive soil. Geotechnique, 34(4), pp. 613-623.
24. Randolph M.F. (2001) personal communication.
25. Rauch A (2003) personal communication.
26. Reese, LC, Cox, WR, and Koop, RD. (1975) "Field testing and analysis of laterally loaded piles in stiff clay," Proc., 7th Offshore Tech. Conf., Houston, pp. 473-483.
27. Whittle, A.J. and Aubeny, C.P. (1993) "The effects of installation disturbance on interpretation of in-situ tests in clays', Predictive Soil Mech., Proc. of the Wroth Memorial Symp., Oxford, England, pp. 742-767.
28. Wood, D.M. (1981) "True triaxial tests on Boston Blue Clay," Proc., 10th Int. Conf. on Soil Mech. and Found. Engrg., pp. 825-830.

UNIT CONVERSION TABLE

Conversion Factors for Different Units of Measurements			
Quantity	SI Unit	Other Unit	Inverse Factor
Length	1m	3.281 feet (ft)	0.3048 m
	1 km	0.540 nautical miles	1.852 km
	1 km	0.6213712 mile	1.609344 km
Area	1 m2	10.764 ft2	0.0929m2
Volume	1 m3	35.315 ft3	0.0283 m3
	1 m3	264.2 gallon (US)	0.00379 m3
	1 m3	220.0 gallon (UK)	0.00455 m3
	1 m3	6.29 barrel (US Petroleum)	0.1589 m3
Velocity	1 m/s	3.281 ft/s	0.305 m/s
	1 m/s	1.943 knot	0.515 m/s
	1 m/s	2.2369 mph	0.44704 m/s
	1 km/hr	0.62137 mph	1.6093 km/hr
Mass	1 kg	2.205 pound	0.454 kg
	1 Mg	0.984 ton (long)	1.016 Mg
	1 Mg	1 tonne (metric)	1 Mg
Force	1 N	0.225 pound force	4.448 N
	1 MN	100.4 ton force	9964 N
	1 MN	224.81 kip	4448 N
	1 kg-force	0.0022046 kip	453.592 kg-force
Pressure	1 N/m2	0.000145 psi	6895 N/m2
	1 kg-force/cm2	0.01422 ksi	70.307 kg-force/cm2
	1 MN/m2	20.885 kip/ft2	47880 N/m2
Energy	1 J	0.738 foot pounds	1.356 J
Power	1 W	0.00134 horsepower	745.7 W
Temperature	00 Celsius	320 Fahrenheit	-17.780 Celsius
Frequency	1 cycle/s	1 hertz	1 cycle/second
Flow Rates	1 m3/day	6.289 barrel/day	0.1589 m3/day
	1 m3/day	35.3146 ft3/day	0.0283 m3/day
Density	1 g/cm3	0.578 oz./inch3	1.73 g/cm3